Materials Transactions, Vol. 65, No. 12 (2024) pp. 1443 to 1457

Raft Structure of Nickel Base Single-Crystal Superalloys*1

Takuma Saito[1,2,*2,*4], Hiroshi Harada[1,*3], Tadaharu Yokokawa[1], Makoto Osawa[1], Kyoko Kawagishi[1,2] and Shinsuke Suzuki[2,3]

[1]*National Institute for Materials Science, Tsukuba 305-0047, Japan*
[2]*Waseda University, Tokyo 169-8555, Japan*
[3]*Kagami Memorial Research Institute of Materials Science and Technology, Tokyo 169-0051, Japan*

Series of Ni-base single-crystal superalloys with superior thermal durability have been developed to improve thermal efficiency of gas turbine systems. Microstructural transition during creep so called "raft structure" formation enhances creep properties at lower stress and higher temperature condition. Furthermore, larger perfection degree of the raft structure contributes to better creep properties under the same creep condition. To control the perfection degree of the raft structure, magnitude of a lattice misfit and an elastic misfit between γ and γ′ phases should be controlled. In the current situation, the lattice misfit can be controlled by using alloy design program NIMS has developed. In this review, we focused on the role of the raft structure in alloy design. Observation results and predicted mechanisms about strengthening by the microstructural transition, in addition to the mechanism about microstructural transition itself during creep, were summarized and explained. Finally, under these recognitions mentioned above, our effort to establish a new alloy design approach to control the perfection degree of the raft structure by modifying the elastic misfit were introduced. [doi:10.2320/matertrans.MT-M2024081]

(Received June 3, 2024; Accepted September 11, 2024; Published November 25, 2024)

Keywords: *Nickel-base single-crystal superalloys, raft structure, elastic misfit, creep strength*

1. Introduction

From the viewpoint of reducing CO_2 emissions and more economical operation, the thermal efficiency of the jet engines and thermal-power-generation is necessary to be improved. Materials which endure high-temperature strength are necessary to use especially at high pressure turbine section because increasing the temperature at the part contributes to higher thermal efficiency. Among all the high-temperature components, turbine blades shown in Fig. 1 are continuously exposed to the most severe environment: higher temperature and pressure originating from burned gas and centrifugal force. Therefore, the development of materials with superior high-temperature strength for turbine blades is important as well as the development of cooling systems and coating systems. Recently, Ni-base single crystal superalloys have been used as a turbine blade material. Companies, universities, and research institutes all over the world are trying to realize the development of Ni-base single crystal superalloys with higher temperature capability. In Japan, National Research Institute for Metals (NRIM) and its successor National Institute for Material Science (NIMS) have been developing a series of Ni-base single crystal superalloys, and it continues to develop new alloys with the highest temperature capability in the world [2–5], shown in Fig. 2. TMS-238, which was developed in 2008, is a hopeful candidate, because it shows high-temperature capability with high oxidation resistance [6]. One of the reasons NIMS has efficiently developed a series of superalloys with better high-temperature strength is that they have developed and used Alloy Design Program (ADP) based on regression analysis from the 1970s, which is significantly earlier than the current trend of materials informatics in the world, and they continue to do alloy design for better creep properties by modifying the microstructure that is predicted by ADP as a function of alloy composition [2, 7].

Fig. 1 Turbine blade made of TMS-138 [1]. (a) One of turbine blades, (b) turbine blades equipped with turbine disc after engine test. With kind permission of IHI Corporation.

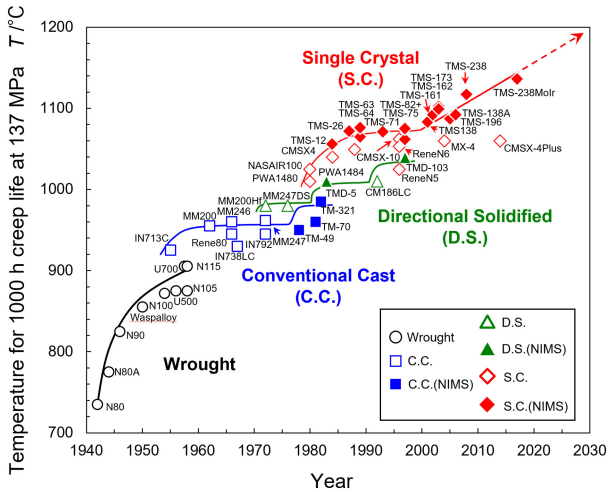

Fig. 2 History of alloy development of Ni-base superalloys [5]. This figure added the data of CMSX-4Plus to original one [5]. Copyright 2021 by The Minerals, Metals & Materials Society. Used with permission.

*1This Paper was Originally Published in Japanese in J. Japan Inst. Met. Mater. **86** (2022) 157–171.

*2Present address: Ruhr-Universität Bochum, Bochum, 44801, Germany
*3Present address: Superalloy Design Laboratory, Tsukuba 305-0031, Japan
*4Corresponding author, E-mail: Takuma.Saito@ruhr-uni-bochum.de

ADP can predict mechanical properties such as creep rupture lives if the composition is input into the ADP [2]. Moreover, predicted creep rupture lives show good agreement with actual experiments, because ADP has been designed to be accurate to the extrapolated values [5]. This high accuracy comes from the accumulation of in-house experimental data with good quality and quantity in addition to establishing regression equations to predict creep rupture lives precisely from the composition. Therefore, for establishing ADP, experimental data in a reliable experimental approach must be collected for a long period, and the relationship between composition and creep rupture lives must be understood experimentally and theoretically. Since establishing ADP needs numerous resources and a longer time, NRIM and NIMS which conduct research from a long-term perspective successfully established the ADP.

Temperature capability T_d (K) with 1000 h creep rupture life is defined as eq. (1), where T_a (K), t_a (h), and C indicate temperature for creep tests, creep rupture life, and material constant which is usually 20, respectively.

$$T_d(C + \log 1000) = T_a(C + \log t_a) \quad (1)$$

At higher temperature and lower stress creep condition such as 1100°C and 137 MPa which is close to temperature capability T_d, the microstructure of Ni-base single crystal superalloy with cubic γ′ precipitates in the γ matrix changes during creep into "raft structure", which is composed of plate-like γ and γ′ phases stacked one after the other. The morphology of the raft structure itself also can continue to change during the creep. It is emphasized that the morphology of the raft structure strongly affects creep behavior at higher temperature and lower stress condition. On the other hand, researchers in this field have not established consensus on evolution mechanisms of the raft structure and the role of the raft structure on the creep behavior regardless of its importance for the alloy design. Therefore, this report summarized previous research about the microstructural evolution of Ni-base single crystal superalloy during creep and the alloy design approach to control the microstructural evolution, including our efforts.

2. Microstructure of Ni-Base Single Crystal Superalloy

This section summarizes the evolution of the microstructure and dislocations during creep at higher temperature and lower stress creep, and its effect on creep behavior.

2.1 Microstructural evolution during creep

Superior high-temperature creep properties of Ni-base single crystal superalloy originate from featured microstructure. Figure 3 shows the typical microstructure of Ni-base single crystal superalloy before the creep. Usually, the microstructure in Fig. 3 is formed after the solution treatment; primary aging at around 1100°C, and secondary aging at around 900°C, respectively. Typical Ni-base single crystal superalloy has γ matrix based on face-centered cubic structure and γ′ precipitates based on $L1_2$ structure in the coherent relation. γ matrix is a solid solution in that alloying elements are distributed randomly in Ni-lattice, while γ′ precipitate is an intermetallic in that alloying elements are distributed regularly.

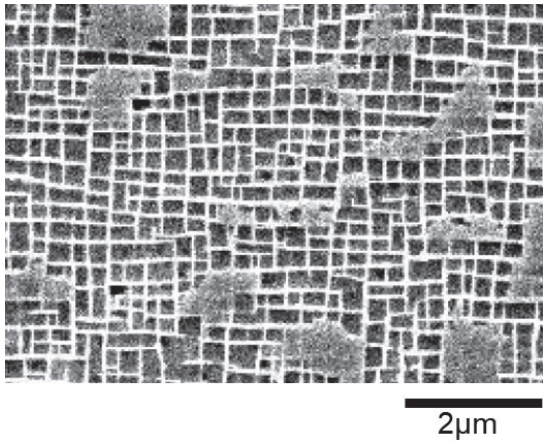

Fig. 3 Microstructure of Ni-base single-crystal superalloy TMS-138 before creep [8]. Gray and black regions indicate γ phase and γ′ phase, respectively. Copyright 2004 by The Minerals, Metals & Materials Society. Used with permission.

Microstructure consisting of γ and γ′ phases changes its morphology during the creep. Figure 4 shows the relationship between a creep curve and microstructure. The preferential growth direction of Ni-base single crystal alloy during directional solidification is along [001], and the longitudinal crystal direction of the turbine blade is also along about [001], therefore, external loading originating from centrifugal force is applied along [001]. To discuss the raft structure formation, γ matrix region which is pallalel to the load direction is called "vertical γ channel", and another γ matrix region which is perpendicular to the load direction is called "horizontal γ channel", respectively to distinguish the relative position of the γ matrix around the γ′ precipitates under the load. Figures 4(b), (c) during primary creep show that the γ′ precipitates are coarsened into the plate like shape perpendicular to the loading direction [001], and the volume of the vertical γ channel is decreased [10, 11]. Raft structure formation decreases creep rate during primary creep, resulting in the transition of the creep stage into secondary creep [9, 12, 13]. Morphology of the raft structure and strain rate are almost maintained during the secondary creep. Therefore, raft structure formation is recognized as a factor to increase creep resistance at higher temperature and lower stress condition such as 1100°C and 137 MPa. As secondary creep proceeds with the accumulation of strain and time, the thickness of γ and γ′ phases in the raft structure becomes larger, and then the wavy morphology of the raft structure appears with a severe increase of strain rate resulting in a collapse of the raft structure [9, 12, 13]. Especially in the Ni-base single crystal superalloy with a high γ′ volume fraction over 50%, "topological inversion" emerges that γ matrix becomes surrounded by the γ′ precipitates during the creep, and γ matrix can be recognized as if it is a precipitate [14, 15]. For instance, the topological inversion is confirmed for the alloys with γ′ volume fraction over 60% in the previous research using tie-lined TMS-82+ with different γ′ volume fraction after creep deformation, shown in Fig. 5. Creep rupture lives of the alloys with 70 and 80% γ′ volume fraction

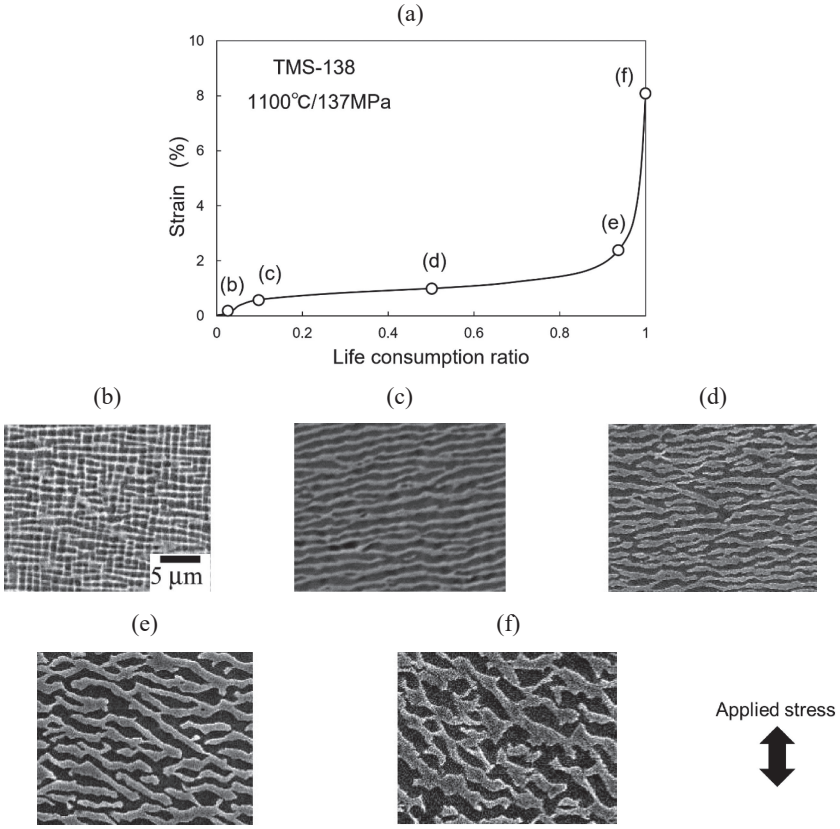

Fig. 4 Relationship between creep curve and microstructure on (100) at 1100°C/137 MPa by using TMS-138 [9]. (a) Creep curve of TMS-138 at 1100°C and 137 MPa, microstructure on (100) at (b) 0.03, (c) 0.1, (d) 0.5, (e) 0.95, (f) 1 in life consumption ratios. Gray and black regions indicate γ phase and γ′ phase, respectively. (a) is adapted from original figure [9]. With kind permission of Trans Tech Publications Ltd.

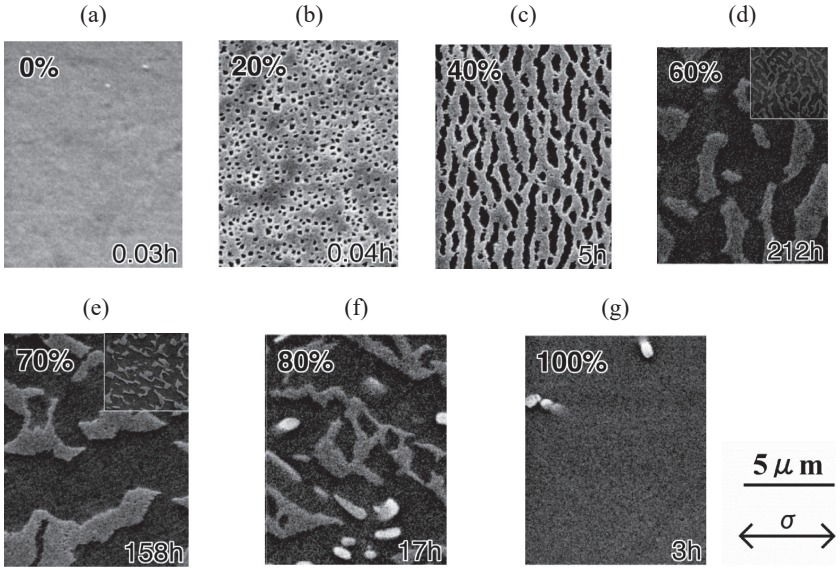

Fig. 5 Microstructure after rupture at 1100°C/137 MPa creep and measured γ′ volume fraction of tie-lined alloys based on TMS-82+ [14]. (a) 0%, (b) 20%, (c) 40%, (d) 60%, (e) 70%, (f) 80%, (g) 100% volume fraction of the γ′ phase. Creep ruptured lives are shown in the right-bottom part of the figures. Gray and black regions indicate γ phase and γ′ phase, respectively. Copyright 2004 by The Minerals, Metals & Materials Society. Used with permission.

tend to be shorter than that with 60% whose kinetic for topological inversion is slower [16].

Raft structure formation enhances the creep resistance at higher temperature and lower stress condition as explained above. However, the raft structure formation does not always show superior mechanical properties in all the creep conditions. At the lower temperature and higher stress condition such as 950°C and 301 MPa, the raft structure is not formed at the minimum creep rate which shows the highest creep resistance, and the increase of the creep rate

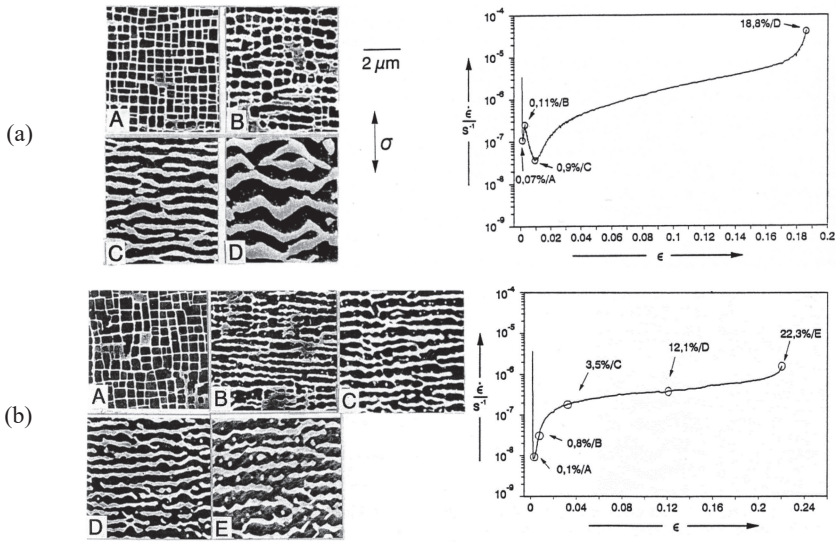

Fig. 6 Microstructure of Ni-base single-crystal superalloy CMSX-4 during creep [13]. (a) 1100°C/140 MPa, (b) 950°C/301 MPa. With kind permission of The Japan Institute of Metals and Materials.

corresponds to the raft structure formation [13], as shown in Fig. 6. Other previous research conducted creep tests at lower temperature and higher stress condition such as 760°C and 793 MPa using specimens with raft structure by conducting the pre-creep at 1100°C and 148 MPa for 50 h and using the specimens without the raft structure. This experiment shows that the specimen with the raft structure show larger creep rate and shorter creep rupture life. Furthermore, in the same report, a difference of the creep rupture lives becomes larger as the applied stress increases using the same specimens with and without the raft structure [17]. According to these previous reports, it should be noted that raft structure formation results in degradation of the creep properties if the creep condition approaches from higher temperature and lower stress into lower temperature and higher stress.

2.2 Evolution of dislocation structure during the creep

Dislocation structure must be paid attention to in addition to the morphology of the microstructure, because the behavior of the line defects, the dislocations, plays a fundamental role in plastic deformation to discuss the creep deformation mechanism of Ni-base single crystal superalloy. Moreover, the formation and the collapse of the raft structure are sometimes affected by the dislocation, therefore, discussion about microstructural evolution cannot rule out the role of the dislocations in these phenomena. In the following section, the dislocation structure observed during the creep at higher temperature and lower stress is explained.

Figure 7 shows the evolution of dislocation structure observed during the creep at higher temperature and lower stress condition such as 1100°C and 137 MPa. Primary creep with raft structure formation shown in Figs. 7(b), (c) shows that dislocations appear in the γ matrix and γ/γ′ interface as a wavy form, but the dislocations inside the γ′ precipitates are hardly observed [18, 19]. Accumulated dislocations at γ/γ′ interface are partly transformed into regular network. From the end of the primary creep until the beginning of the secondary creep with the formation of the raft structure, dislocations such as $\frac{1}{2}a[101]$, $\frac{1}{2}a[10\bar{1}]$, $\frac{1}{2}a[011]$, and $\frac{1}{2}a[01\bar{1}]$ types are accumulated [18, 19] and formed at the horizontal γ/γ′ interface in the raft structure [20, 21]. Inside the γ′ precipitates, a pair of dislocations with straight form becomes multiplicated, and these dislocations are recognized as a pair of the dislocation with anti-phase boundary (APB) in the types of $\frac{1}{2}a[101]$, $\frac{1}{2}a[10\bar{1}]$, $\frac{1}{2}a[011]$, and $\frac{1}{2}a[01\bar{1}]$ with equivalent Schmidt factor of $\frac{1}{2}a[101]$ [18, 19]. Except for the pair of the dislocations mentioned above, uniaxial tensile creep sometimes causes $a\langle 100\rangle$ type dislocations with compact core structure in the γ′ precipitates, and similar dislocations are reported in the type of $a[001]$ [22] and $a[100]$ [23] dislocations. $a[100]$ dislocations can cross the γ′ precipitates as if they connect the faced γ/γ′ interfaces as shown in Fig. 8(a), and they are connected to $\frac{1}{2}a[011]$ or $\frac{1}{2}a[01\bar{1}]$ interfacial dislocations [22, 23] as shown in Fig. 8(b).

3. Microstructure and Creep Deformation Mechanism

The creep behavior of Ni-base single crystal superalloy is affected by morphological evolution of the microstructure such as the formation and the collapse of the raft structure. At higher temperature and lower stress condition, raft structure formation enhances creep resistance. Furthermore, stable raft structure during the creep delays the collapse of the raft structure resulting in longer creep rupture life. Creep deformation mechanisms from the beginning of the raft structure formation to its collapse are described in the following part from the viewpoints of dislocation theory at higher temperature and lower stress condition. To enhance the temperature capability, understanding deformation mechanism at this condition such as 1100°C/137 MPa is essential.

3.1 Microstructure after standard heat treatments

Generally, heat treatments of Ni-base single crystals consist of three steps; solution treatment, primary aging treatment, and secondary aging treatment. The solution treatment aims to remove eutectic γ′ phases precipitated during the solidification process and decreases the solidified

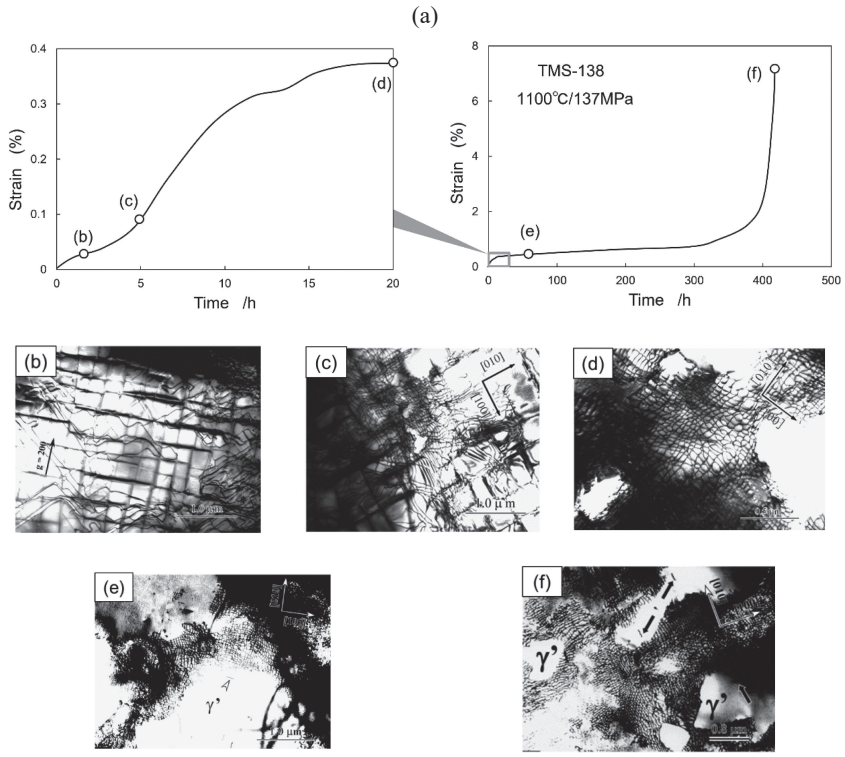

Fig. 7 Relationship between creep curve at 1100°C/137 MPa and dislocation structure on (001) by using TMS-138 during creep and after creep rupture [18, 19]. TEM foil is normal to the applied stress direction. (a) Creep curve of TMS-138 at 1100°C/137 MPa [18], (b) 2 h interruption showing cross slipped dislocations in the horizontal γ channel [18], (c) 5 h interruption showing the interfacial dislocation network appears on the horizontal γ/γ′ interface [18], (d) 20 h interruption showing developed interfacial dislocation network covers horizontal γ/γ′ interface [18], (e) 60 h interruption showing superdislocations in the γ′ phase with short and straight shape [18], (f) after rupture showing superdislocations in the γ′ phase with short and straight shape [19]. (a) is adapted from original figure [18]. Reprinted from publications [18, 19] with permission from Elsevier.

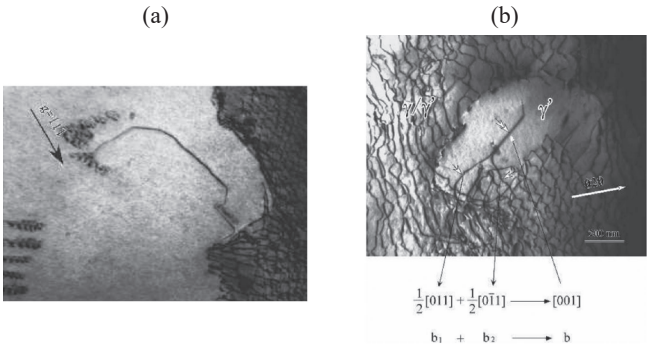

Fig. 8 *a*[001] dislocation in γ′ precipitates after creep rupture at 1150°C/137 MPa using TMS-138 [22]. (a) *a*[001] dislocation connected with two γ/γ′ interfaces, (b) *a*[001] dislocation connected with interfacial dislocations on the horizontal γ/γ′ interface. The TEM foil is normal to the applied stress direction. Reprinted [22] by permission from Springer Nature.

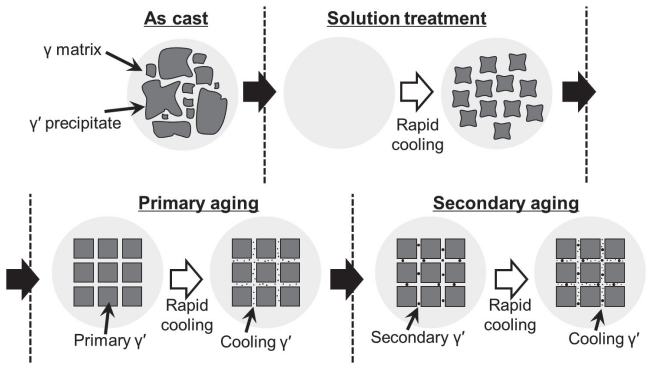

Fig. 9 Microstructural evolution during standard heat treatment in actual Ni-base single-crystal superalloys [24, 25]. This figure is adapted from original one [24] to indicate more detailed microstructural transition in Ni-base single-crystal superalloys with a high volume fraction. With kind permission of Dr. Akihiro Sato [24].

segregation. Primary aging treatment reproduces the heat history which is equivalent to that of thermal spray coating to the surface of the turbine blades. Secondary aging treatment usually aims to causes strengthening the part exposed to lower temperature and relieve the internal stress to escape from cracking in the process of fluorescent flaw detection. Figure 9 summarizes the relationship between heat treatment processes and the microstructure of Ni-base single crystal superalloy. Aligned-cubic γ′ precipitates shown in Fig. 3 appear during the primary aging, and coarsening of the secondary γ′ precipitates could be observed during secondary aging. This chapter focuses on the primary aging which determines the distribution and the shape of the γ′ precipitates.

The lattice constant of the γ and γ′ phases are different from each other due to the difference in the order-disorder structure and the compositions. Therefore, as the coherent γ/γ′ interface is kept, the local elastic stress field around γ/γ′ interface appears, defined by the eq. (2) called lattice misfit, where a_γ and $a_{\gamma'}$ are lattice constant of the γ and γ′ phases, respectively. Almost all the commercial Ni-base single crystal superalloys have larger thermal expansion coefficients of the

γ phase than that of the γ′ phase [26, 27], and this physical feature results in a negatively larger lattice misfit as the temperature increases. Under the primary aging around 1100°C, γ′ precipitates become aligned-distributed and cubic shape due to negatively larger lattice misfit. The formation of cubic γ′ precipitates comes from that a contribution of the strain energy by the lattice misfit is larger than that of the chemical-interfacial energy to the overall free energy in case of a negatively larger lattice misfit. In addition, regular distribution of cubic γ′ precipitates is caused by the elastic interaction by neighbored γ′ precipitates [28–30]. Furthermore, γ/γ′ interfaces of cubic γ′ precipitates are usually on {100} due to anisotropy of the elastic modulus between along ⟨100⟩ and ⟨111⟩ in the surrounding γ matrix [31].

$$\delta_L = \frac{a_{\gamma'} - a_{\gamma}}{a_{\gamma}} \tag{2}$$

3.2 Primary creep and formation of the raft structure

Higher temperature and lower stress creep condition activates the climb motion of the dislocations rather than the slip motion typically activated at lower temperature and higher stress creep condition, and almost all the dislocations move in the γ matrix or along the γ/γ′ interface. During the primary creep, $\frac{1}{2}a[101]$, $\frac{1}{2}a[10\bar{1}]$, $\frac{1}{2}a[011]$, and $\frac{1}{2}a[01\bar{1}]$ dislocations move as slip and climb motion in the γ matrix in addition to the diffusion of the solute elements via vacancy motion which is an elementary kinetic step for the raft structure formation. Both factors of dislocation motion and atomic diffusion contribute to the strain emerging in the primary creep [8]. Raft structure formation reduces the volume of the vertical γ channels which are parallel to the loading direction, and the pathway in the γ matrix for $\frac{1}{2}a[101]$, $\frac{1}{2}a[10\bar{1}]$, $\frac{1}{2}a[011]$, and $\frac{1}{2}a[01\bar{1}]$ dislocations is blocked by coarsened γ′ precipitates with the raft structure [10, 11]. A decrease of vertical γ channels suppresses the slip and climb motion of those dislocations, and contributes to the decrease in the creep rate, and then, secondary creep appears [11]. With the formation of the raft structure, a regular dislocation network is gradually formed on the horizontal γ/γ′ interface, and this dislocation network itself also contributes to the appearance of the secondary creep. Repulsive force from the dislocation network to approaching dislocations in the γ matrix [19], and larger stress for the entering dislocations in the γ matrix into γ′ precipitates across the dislocation network to pass through spacing in the dislocations network can explain the contribution of the dislocation network to the strengthening [20].

In the creep deformation of Ni-base single crystal superalloy consisting of coherent γ and γ′ phases, the internal elastic strain field becomes highly complex because the local elastic strain field appears originating from loading and the dislocations in addition to the lattice misfit. Moreover, the elastic strain field itself continues to be changed during the creep. This local elastic strain is assumed to be a main factor in forming the raft structure during the creep at higher temperature and lower stress condition. Figure 10 summarizes the mechanism for the raft structure formation focusing on the local elastic strain, and shows the relationship between local elastic strain and microstructure during creep. The mechanisms for the raft structure formation are mainly categorized into “elastic stage [10, 32]” in which dislocations never contribute to the raft structure formation and “elastic-plastic stage [33]” in which dislocations play a fundamental role in the raft structure formation. Before the creep deformation shown in Fig. 10(a), elastic strain caused by the lattice misfit locally exists around γ/γ′ interface, and the elastic strain is mainly parallelly distributed along the γ/γ′ interface. Focusing on the elastic strain parallel to the γ/γ′ interface, the elastic strain is isotropically distributed in the γ matrix around the γ′ precipitates. Hereafter, detail of the elastic stage and elastic-plastic stage in the mechanism of the raft structure formation is explained, focusing on the evolution of the elastic strain parallel to the γ/γ′ interface.

3.2.1 Elastic stage

The difference of the physical parameters between γ and γ′ phases is not only confirmed in the lattice constant, but also in the elastic constant. In a case of ⟨100⟩ longitudinal elastic

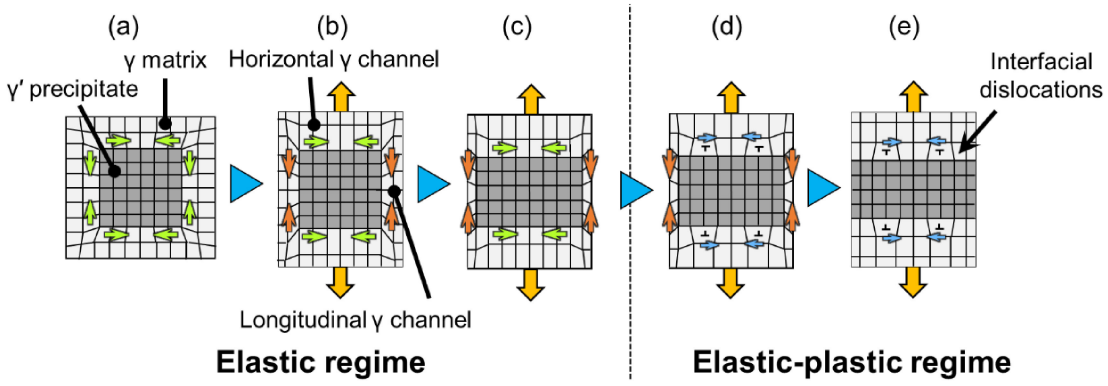

Fig. 10 Evolution of internal elastic strain field caused by the coherent γ/γ′ interface and morphology of microstructure [34]. (a) Elastic regime before creep, (b), (c) elastic regime during creep, (d), (e) elastic-plastic regime during creep. This schematic illustration assumes conventional Ni-base single-crystal superalloy with negative lattice misfit defined by eq. (2) and positive elastic misfit defined by eq. (3). Furthermore, the elastic strain caused by the misfits indicated by arrows inside of microstructure is assumed to be applied only in the γ matrix. Elastic strain indicated by arrows inside the microstructure is stronger in orange, green, and blue, in this order. It should be noted that actual elastic strain in each region must take contribution of external applied stress into consideration, in addition to contribution of the coherent γ/γ′ interface shown in this figure. This figure was modified to show the internal elasticity field for more easily understanding from original one [34]. Copyright 2021 by The Minerals, Metals & Materials Society. Used with permission.

modulus in actual-used Ni-base single crystal superalloys, the value of the γ′ phase tends to be larger than that of γ phase, and the elastic misfit defined by the eq. (3) is usually positive.

$$\delta_E = \frac{E_{\gamma'}^{\langle 100\rangle} - E_{\gamma}^{\langle 100\rangle}}{E_{\gamma}^{\langle 100\rangle}} \tag{3}$$

In Ni-base single crystal superalloy with positively larger elastic misfit and negatively larger lattice misfit, elastic elongation by the loading is larger in γ matrix than that in γ′ precipitates, under the assumption that the same applied stress is distributed to all the consisting regions of microstructure. If a geometric difference emerges by the difference of the elastic elongation from the elastic misfit, the smallest unit of the microstructure as shown in Fig. 10(a) cannot be maintained. To compensate for the gap by the elastic misfit keeping the coherency between γ and γ′ phases, a new elastic strain parallel to the γ/γ′ interface along the loading direction has to be caused [34, 35]. By appearing the new elastic strain caused by the elastic misfit during the loading, the elastic strain field along the γ/γ′ interface becomes more anisotropic, and the elastic strain in the vertical γ channel becomes larger in the compressive side along the loading direction. As this result, the elastic stress field becomes also anisotropic, and the resolved shear stress in the vertical γ channel is smaller than that in the horizontal γ channel [36]. Due to this distribution, dislocations which enter vertical γ channel cannot obtain enough large resolved shear stress for the motion, and the vertical γ channel itself is also considered to be an obstacle for the dislocation motion. Furthermore, the anisotropic elastic stress field affects the distribution of the dislocations in the γ matrix, for instance, 60° degree dislocations of $\frac{1}{2}a[101]$, $\frac{1}{2}a[10\bar{1}]$, $\frac{1}{2}a[011]$, and $\frac{1}{2}a[0\bar{1}1]$ types preferentially appear in the horizontal γ channel, but screw dislocations of $\frac{1}{2}a[101]$, $\frac{1}{2}a[10\bar{1}]$, $\frac{1}{2}a[011]$, and $\frac{1}{2}a[0\bar{1}1]$ types preferentially appears in the vertical γ channel [37, 38].

The anisotropic elastic strain field along the γ/γ′ interface is not only a factor to cause anisotropy of dislocation motion, but also a fundamental factor to form the raft structure. Under the assumption in Fig. 10(b), elastic strain parallel to the γ/γ′ interface which is necessary for the coherency is larger in the vertical γ channel than that in the horizontal γ channel, and the γ/γ′ interface along the vertical γ channel can be regarded as a relatively unfavorite site from the viewpoint of the elastic energy. Therefore, to remove such an unfavorable region to decrease the total free energy in the system, the raft structure is formed as shown in Fig. 10(c). At the beginning of the raft structure formation, anisotropy of the elastic strain parallel to the γ/γ′ interface can be a trigger to change the distribution of chemical potential of constituent elements between vertical and horizontal γ channels [39, 40]. Then, the raft structure begins to be formed by inter-diffusion of elements via vacancy motion between vertical and horizontal γ channels [39, 40]. In the process of atomic diffusion, γ former elements such as Cr and Mo are reported to move from vertical γ channel into horizontal γ channel as shown in the previous research [41–43].

3.2.2 Elastic-plastic stage

The dislocation density in the γ matrix becomes gradually larger by the activity of the dislocation source from the beginning to the end of the primary creep, although the recovery process by diminishing the dislocations should be also considered more strictly. Since the dislocations themselves have the elastic strain field around their core, they can relax the coherent elastic strain on the horizontal γ/γ′ interface in the raft structure originating from the lattice misfit by their accumulation on the interface. Later, accumulated dislocations are transformed into the regular dislocation networks such as squire [21, 37, 44, 45], wavy [18, 21], a combination of octagonal and squire shape [20, 21], and hexagonal shape [21] to more efficiently relax the coherent strain [20] by changing dislocation line directions and dislocation reaction such as transition of Burger's vector from $\frac{1}{2}a[101]$ into $\frac{1}{2}a[110]$, $a[100]$ or $a[001]$. By the development of the dislocation network with the accumulation of the dislocations on the horizontal γ/γ′ interface, the elastic strain field in the γ matrix surrounding γ′ precipitates becomes more anisotropy, and the elastic strain along the γ/γ′ interface in the vertical γ channel is considered to be larger than that in the horizontal γ channel. This further enlarges the driving force for the raft structure formation [33, 46], and facilitates the formation of the raft structure, as shown in Fig. 10(e). Moreover, the atomic diffusion is accelerated around the dislocation core due to pipe-diffusion, and the kinetic for the raft structure formation is accelerated by active pathway for the pipe-diffusion of the horizontal γ/γ′ interface with the dislocation network [47].

3.3 Secondary, tertiary creep and collapse of the raft structure

Figures 4 and 6(a) show that the thickness of the γ and γ′ phases in the raft structure gradually increases from the secondary creep to tertiary creep. Thickening implies the motion of the horizontal γ/γ′ interface and decreases the net areal density of the γ/γ′ interface in the whole specimen [48]. Since the dislocation networks form on the horizontal γ/γ′ interface in the raft structure, decreasing the arial density of the γ/γ′ interface is coincident with decreasing the dislocation density in the whole specimen which could be equivalent to the recovery process in the secondary and tertiary creep. The recovery phenomenon to decrease the density of the dislocation network mentioned above is caused by the $a\langle 100\rangle$ dislocation shearing raft-γ′ precipitates [22, 23, 49–53] shown in Fig. 8, and it results in the rate-controlling mechanism in secondary creep [23, 51, 53]. A detailed recovery mechanism is proposed that the motion of $a\langle 100\rangle$ dislocation in the γ′ phase in the raft structure disappears the connected dislocations such as $\frac{1}{2}a[101]$, $\frac{1}{2}a[10\bar{1}]$, $\frac{1}{2}a[011]$, and $\frac{1}{2}a[0\bar{1}1]$ types in the γ matrix, and then activates the motion of the other dislocations in the γ matrix [23]. $a\langle 100\rangle$ dislocation reaching the opposite γ/γ′ interface across the rafted γ′ precipitates disappears a part of reached $a\langle 100\rangle$ dislocation, and this also can be acted as a recovery process [50, 51]. The core structure of $a\langle 100\rangle$ dislocations consists of closely separated dislocations $\frac{1}{2}a\langle 101\rangle$ types on different $\{111\}$, and the pair keeps a constant distance taking the glide and climb motion, again and again [49, 51, 53]. And then, the total Burger's vector is $a\langle 100\rangle$ at the larger scale, but closely separated dislocations with different Burger's vector ex-

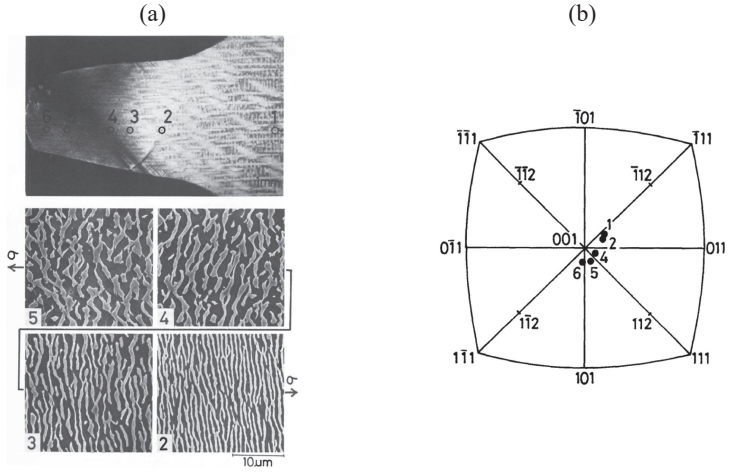

Fig. 11 Creep ruptured specimen of Ni-base single-crystal superalloy TMS-12 at 1040°C/137 MPa [54]. (a) Slip bands and microstructure, (b) lattice rotation. Gray and black regions indicate γ phase and γ′ phase, respectively. Copyright 1984 by The Minerals, Metals & Materials Society. Used with permission.

change the vacancies which is necessary for the climb motion with each other at the smaller scale [49, 51, 53].

Figure 4 and Fig. 6(a) also show the thickening of the raft structure accompanies the waving of the raft structure. For instance, after the creep rupture shown in Fig. 11(a), a wavy raft structure is also more frequently observed as the observed region approaches to the ruptured surface [54]. However, the detailed mechanism to cause the wavy form of the raft structure is still necessary to investigate. An optical microscope observation in the dark field mode indicates that black lines are observed in the region with the wavy raft structure in Fig. 11(a) [54]. One directed black line is observed in the region with an inclined raft structure in one direction at the position of "4" in Fig. 11(a), but two directed black lines are observed in the region with the wavy raft structure at the position of "5" in Fig. 11(b). The region with black lines is considered to be homogenous slip lines because the region crosses the whole specimen with a straight shape and inclined to the longitudinal direction to the specimens in the two directions. Before and after the passing through the region with black lines, lattice rotation appears as shown in Fig. 11(b), and this implies that active dislocation motion which develops the homogenous slip lines in a vast region facilitates to wave the raft structure. From the viewpoint of the pure elastic theory which does not consider the shearing of the γ′ phase in the raft structure by dislocations, wavy raft structure can be simulated using elastic energy calculation [55] and phase field approach [56] under the assumption that excess dislocations are deposited only in the γ matrix and high plastic strain. However, since the dislocations also moves in γ′ phase in the raft structure combining with their motion in the γ matrix, there is a room to establish the new view for describing the mechanism of the waving. In summary, the role of the dislocations in waving the raft structure has not been fully clarified, therefore, this topic is necessary to be addressed.

The topological inversion that can occur in the alloys with high γ′ volume fraction requires thermal equilibrium conditions to minimize the interfacial energy [57]. This process is reported to be accompanied by the massive solute diffusion near the dislocation core in the γ′ precipitates [15, 58].

The collapse of the raft structure including thickening, waving, and topological inversion needs the motion of the γ/γ′ interface in the raft structure in all the cases. In addition, the dislocation networks on the γ/γ′ interface are also required to be moved. In this process, interfacial dislocations take a climb motion, therefore, the kinetic of the motion of the γ/γ′ interface decreases by the existence of the interfacial dislocations [28]. Heavy elements segregated to the γ/γ′ interface could also decrease the kinetic of the motion of the γ/γ′ interface [28, 59, 60].

4. Alloy Design Approach to Control Perfection Degree of the Raft Structure

To develop the Ni-base single crystal superalloys with superior temperature capability, microstructure which contributes to strengthening is necessary to be controlled. In actual-used Ni-base single crystal superalloys, a particularly significant microstructure to be controlled is the dislocation network and the raft structure. For instance, as the spacing on the dislocation network decreases, a larger repulsive force to the approaching dislocation can be obtained [19]. In addition, larger stress to enter into γ′ precipitates from γ matrix is required to pass through the spacing between the dislocation network [20]. Moreover, the denser dislocation network could contribute to delaying the collapse of the raft structure due to the slower motion of the dislocation network itself [28]. To obtain the denser dislocation network, the composition should be modified so as to negatively increase the lattice misfit [20]. On the other hand, the morphology of the raft structure immediately after its formation should be controlled if the target microstructure in the alloy design is the raft structure. What is the ideal morphology of the raft structure, and how should the morphology be controlled?

4.1 Perfection degree of the raft structure and creep properties

A perfection degree of the raft structure which is often

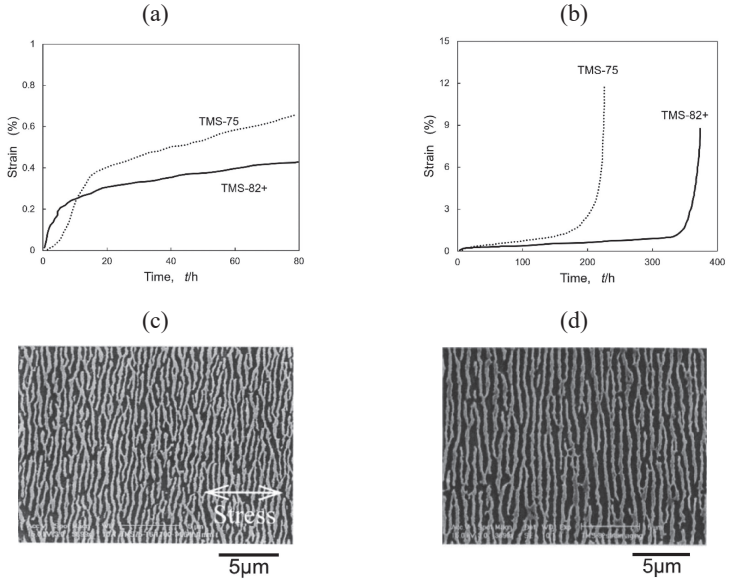

Fig. 12 Relationship between creep curves at 1100°C/137 MPa and microstructure interrupted at 64 h in the secondary creep [62]. (a) Primary creep, (b) entire creep curves, (c) microstructure interrupted at 64 h in TMS-75, (d) microstructure interrupted at 64 h in TMS-82+. Gray and black regions indicate γ phase and γ′ phase, respectively. (a) and (b) are adapted from original figures [62]. Copyright 2000 by The Minerals, Metals & Materials Society. Used with permission.

defined as an aspect ratio of the γ′ precipitates in the raft structure that can be determined by the smoothness of the horizontal γ/γ′ interface and continuity of γ′ precipitates, is an indicator for the microstructural control for the alloy design at higher temperature and lower stress creep conditions. The perfection degree becomes larger, and the creep resistance is enhanced if the horizontal γ/γ′ interface is smoother and the γ′ precipitates perpendicular to the loading direction is more continuous. A higher perfection degree means that larger net area of the horizontal γ/γ′ interface [61] and a smaller volume of the vertical γ channel which is a pathway for the dislocations. For instance, Fig. 12 shows the relationship between creep curve and microstructure of TMS-75 and TMS-82+ [62]. Immediately after the formation of the raft structure, the perfection degree of the raft structure in TMS-82+ is larger than that in TMS-75, which is coincident with the trend that TMS-82+ shows higher creep resistance: smaller creep rate during secondary creep and longer creep life [62–64].

4.2 Perfection degree of the raft structure and mechanism of the microstructural evolution

The perfection degree of the raft structure can be mainly controlled by the initial distribution of the γ′ precipitates before the creep and the kinetic for the raft structure formation. How the above factors affect the perfection degree of the raft structure is described in the following chapter.

4.2.1 Initial distribution of the γ′ precipitates

Figure 13 compares the microstructure of Ni-base single crystal superalloys NASAIR100 and Alloy F before and after the creep tests. Figure 13 shows the alloy with regularly distributed and cubic γ′ precipitates before the creep tends to show the higher perfection degree of the raft structure. For instance, NASAIR100 in Fig. 13(a) shows regularly distributed and cubic γ′ precipitates, while Alloy F in Fig. 13(b) shows randomly distributed and spherical γ′ precipitates. This difference in the initial microstructure comes from the difference of the lattice misfit, for instance, the lattice misfit of NASAIR100 at 1000°C is approximately −0.45% [26], on the while, that of Alloy F is assumed to be approximately 0 [28]. Negatively larger lattice misfit contributes to the larger elastic interaction between neighboring γ′ precipitates, resulting in the regular distribution of the γ′ precipitates. Furthermore, if the lattice misfit moves to negatively larger values from 0, γ′ precipitates tend to be a cubic shape from spherical shape because the ratio of the strain energy to the chemical surface energy in the total free energy becomes larger. Creep tests at 1000°C and 148 MPa using both alloys show that the perfection degree of the raft structure of NASAIR100 shown in Figs. 13(b), (c) is larger than that of Alloy F shown in Figs. 13(c), (f). This might be because the direction of the neighboring γ′ precipitates and that of coarsening to form the raft structure are coincident with each other in the initial microstructure with the regularly distributed and cubic γ′ precipitates, resulting in the higher perfection degree of the raft structure [28]. In summary, the raft structure with a higher perfection degree can be expected if the lattice misfit is modified into a further negatively larger one in the alloy design focusing on the initial microstructure before the creep.

4.2.2 Kinetics for the raft structure formation

If the raft structure forms rapidly and the primary creep emerges earlier, the perfection degree of the raft structure tends to be larger [62], such as in the case of TMS-82+ shown in Fig. 12. In such a case, less dislocations can enter the vertical γ channel. On the other hand, some dislocations can enter the vertical γ channel if the kinetic for the raft structure formation is slow [23] such as in the case of TMS-75, that could form the dislocation network on the vertical γ/γ′ interface and relax the coherent strain caused by the lattice and the elastic misfit under loading. If the elastic strain along the γ/γ′ interface is relaxed on the vertical γ/γ′

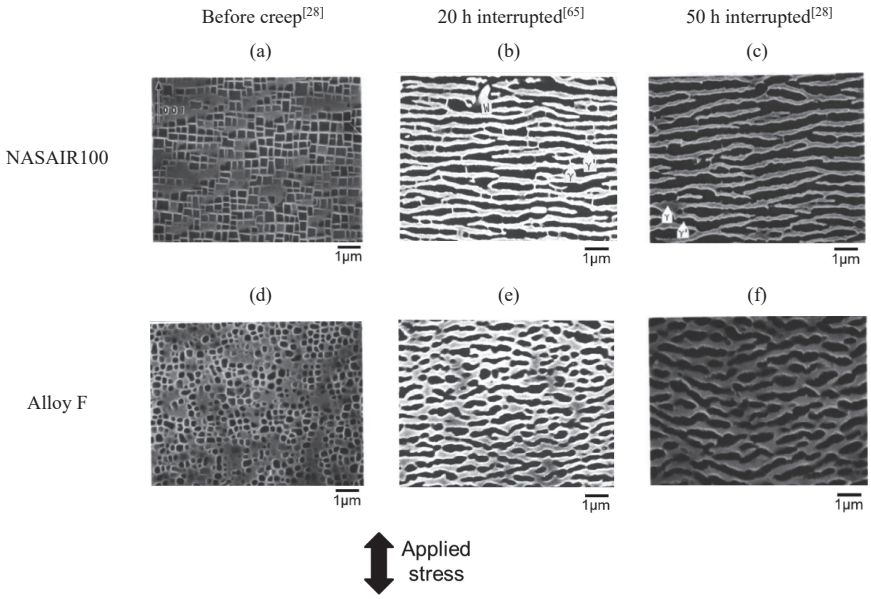

Fig. 13 Effect of the lattice misfit on microstructure creeped at 1000°C/148 MPa [28, 65]. Lattice misfit of NASAIR100 is approximately −0.45% [26], while that of Alloy F is expected to be approximately 0% at 1000°C [28]. Gray and black regions indicate γ phase and γ′ phase, respectively. Reprinted from publication [28] with permission from Elsevier. Reprinted [65] by permission from Springer Nature.

interface, the anisotropy of the strain along the γ/γ′ interface is reduced, resulting in a decrease of the driving force for the raft structure formation. Therefore, the kinetics for the raft structure formation should be enlarged to obtain the higher perfection degree of the raft structure, and enlarging the driving force for the raft structure formation can be effective. To complete the raft structure before the entry of the dislocations into the vertical γ channel, the elastic stage which assumes a smaller dislocation density in the mechanism of the raft structure formation is focused on. The driving force for the raft structure formation in the elastic stage originates from the elastic misfit during the loading, and it is assumed to be enlarged if the elastic misfit is modified into further positively larger one in the case of actual-used Ni-base single crystal superalloys.

The experimental results supporting above hypothesis is shown in Fig. 14. More dislocations on the γ/γ′ interface before the creep are confirmed as the temperature at the primary aging is above 1120°C, as shown in Figs. 14(e), (f) [66]. This phenomenon can be explained by the negatively larger lattice misfit at higher temperature in the primary aging. Since the conventional Ni-base single crystal superalloys have the negatively larger lattice misfit and its value increases as the temperature increases [26, 27], the elastic strain parallel to the γ/γ′ interface originating from the lattice misfit also increases. When the lattice misfit becomes enough negatively larger that cannot maintain coherency, many dislocations are introduced on all the γ/γ′ interface surrounding γ′ precipitates to relax the excess coherent strain by the transition from coherent interface into "semi-coherent" interface. Creep tests using a series of specimens with different conditions of the primary creep at 1100°C and 137 MPa, the perfection degree of the raft structure decreases resulting in shorter creep rupture lives as the temperature in the primary aging becomes higher. Different from the case with coherent γ/γ′ interface, semi-coherent interface can be assumed to have weak restriction to maintain the coherency during the loading that is caused by the geometrical difference of the elastic elongation between the phases originating from the elastic misfit. Therefore, anisotropy of the elastic strain parallel to the γ/γ′ interface becomes smaller, resulting in the smaller driving force for the raft structure formation and the smaller perfection degree of the raft structure.

According to Hooke's law, the relationship between the elastic strain and the applied stress is proportional. Therefore, under the assumption that the same applied stress is distributed equally to all the regions, larger applied stress causes a larger geometrical difference in the elastic elongation between the γ′ phase and vertical γ channel by the elastic misfit. In this situation, the larger elastic strain towards the compressive side to the more elongated phase is necessary to maintain the coherency between the phases. In the elastic stage of the raft structure formation mechanism, larger applied stress contributes to the larger anisotropy of the elastic strain parallel to the γ/γ′ interface, resulting in the faster formation of the raft structure [64]. However, it should be noted that the kinetics for the raft structure formation is also affected by the diffusion kinetics of the solute elements because the raft structure formation needs atomic diffusion via vacancy motion under the presence of the driving force for the raft structure formation. Moreover, diffusion of solute elements itself also contributes to the creep deformation, especially at higher temperature such as a situation that the raft structure is forming. In a case shown in Fig. 12, TMS-75 contains two times larger Re whose diffusion rate is the slowest in the conventional superalloys than that of TMS-82+. Figure 12 shows that the primary creep of TMS-75 emerges more slowly than that of TMS-82+, and this phenomenon can be explained by both of the slower diffusion rate and smaller driving force for the raft structure formation.

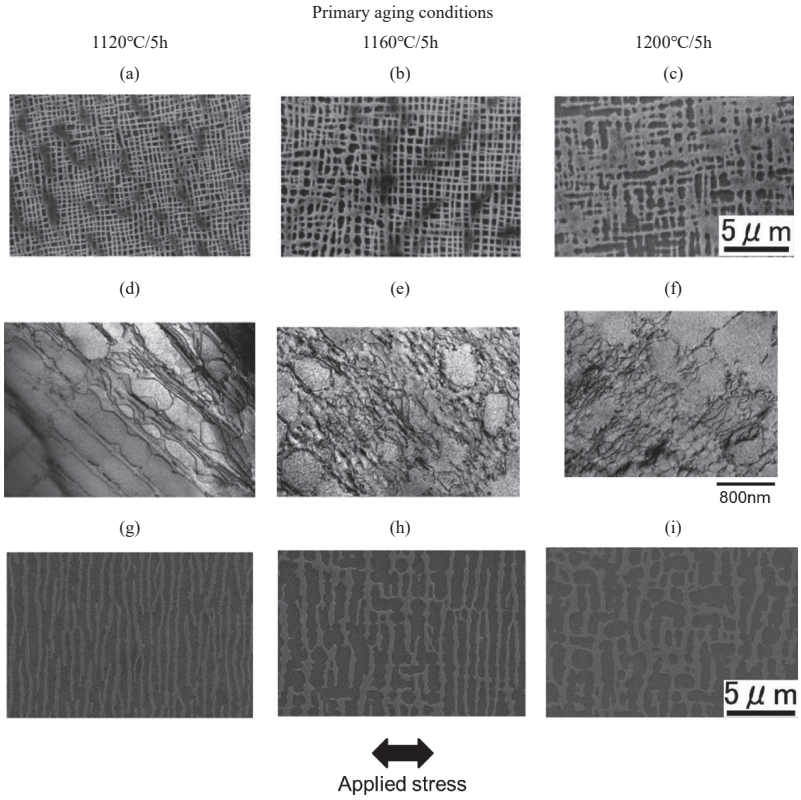

Fig. 14 Effect of primary aging conditions on microstructure of Ni-base single-crystal superalloys TMS-26 [66]. (a)–(c) SEM images before creep, (d)–(f) TEM images before creep, (g)–(i) SEM images after creep ruptured at 1100°C/137 MPa. Creep ruptured lives were 351, 116 and 62 h when primary aging conditions were 1120°C/5 h, 1160°C/5 h and 1200°C/5 h, respectively. Gray and black regions indicate γ phase and γ′ phase in SEM images, respectively. Indicated applied stress direction refers to (g)–(i). With kind permission of The Japan Institute of Metals and Materials.

In summary, the raft structure with a higher perfection degree can be expected if the elastic misfit is modified into a further positively larger one in the alloy design focusing on kinetics for the raft structure formation.

5. Prediction of the Elastic Misfit

To obtain the higher perfection degree of the raft structure in the alloy design, as mentioned above, aligned cubic γ′ precipitates in the initial microstructure by negatively enlarging the lattice misfit, and larger kinetics for the raft structure formation by positively enlarging the lattice misfit are effective, respectively. NIMS has developed the predictive equations of the lattice misfit in a function of the concentration of the alloying elements and temperatures, and they are installed into the ADP. This enables the alloy design to control the lattice misfit and NIMS has developed a series of Ni-base single crystal superalloys with higher perfection degree of the raft structure and denser dislocation networks. However, ADP has a room to be improved in its accuracy, because the elastic misfit that is a main factor to control the perfection degree of the raft structure has not been derived as equations using regression analysis and such equations have not been installed to ADP yet. Therefore, we established predictive equations of the ⟨100⟩ longitudinal elastic modulus of the individual γ and γ′ phases, and then the elastic misfit at the equilibrium compositions between the phases is estimated with the use of the equilibrium equations installed into ADP [2, 7, 67], aiming for the use of new alloy design approach. First of all, we were trying to establish the predictive equations of the elastic modulus of the individual γ and γ′ phases using regression analysis in experimentally obtained elastic modulus, as in the similar approach to establish the predictive equation of the lattice misfit [34].

To establish the regression equations in functions of temperature and concentration of the alloying elements, the amount of experimental data has to be over the numbers of all the functions. However, previously reported elastic modulus of Ni-base superalloy adapting to the individual γ and γ′ phases is limited, and the reported elastic modulus was measured by the various methods. Therefore, we had to measure the elastic modulus of a series of Ni-base alloys using the unified method.

5.1 Method to measure the elastic modulus

The experimental approach to measure the elastic modulus is roughly categorized into static tests and dynamic tests, and the elastic strain rate of the specimen during measurement in the dynamic tests is faster than that in the static tests. The static tests refer to the mechanical test, including the hardness test, tensile test, and compressive test. Measured elastic modulus by the static tests could show strain-rate dependency affected by the viscoelasticity of the specimen since the elastic strain rate is slower than that of dynamic tests. The dynamic tests refer to ultrasound tests and resonance tests, for instance, pulse-echo method, bar-resonance method, and

rectangular parallelepiped resonance (RPR) method. Since the elastic strain rate in the dynamic tests is faster than that of the static tests, the obtained elastic modulus is less affected by the viscoelastic properties of the specimens. Therefore, the dynamic tests are favorable to obtain pure elastic modulus without viscoelasticity. On the other hand, the pulse-echo method is difficult to measure the elastic modulus at higher temperatures, because the measured elastic modulus can be easily affected by the surface state, which is oxidized at higher temperatures. Bar-resonance method needs relatively larger specimens, therefore, elastic modulus measurement is not suitable for the Ni-base single crystal superalloys which need much cost. We used RPR method [68–70] to measure the elastic modulus, because small rectangular specimens with approximately 4 mm edge can be used and the method can measure the elastic modulus of the bulk specimen instead of the surface. We measured the elastic modulus of a series of Ni-base single crystal alloys with the individual γ and γ′ phases using the RPR method between room temperature and 1100°C.

5.2 Predictive equations of the elastic modulus by regression analysis

Figure 15 shows the ⟨100⟩ longitudinal elastic modulus of γ single-phase alloys obtained by the RPR method, and Fig. 16 shows those of γ′ single-phase alloys [34]. ⟨100⟩ longitudinal elastic modulus of the γ single-phase alloys more greatly decreases with an increase of temperature than those of γ′ single-phase alloys. This trend implies that the elastic misfit defined by eq. (3) could be positively larger as the temperature increases, in a similar manner to the lattice misfit. Notably, the elastic modulus of pure Ni as a γ single-phase alloy was not obtained due to the magnetostriction [71] between room temperature and 358°C, which is the Curie temperature of pure Nickel.

Regression analysis using measured elastic modulus by RPR method and referenced ones of Ni-Al system by the same method was conducted in the eq. (4), where T, c_i, A_i, and D_x indicate temperature, the concentration of i-th element, a product of T and c_i, and regression coefficient of function x, respectively. Notably, the term of Al c_{Al} in γ′ phase is expressed as $25 - c_i$ to put the starting point Ni_3Al. The regression analysis can determine the values of

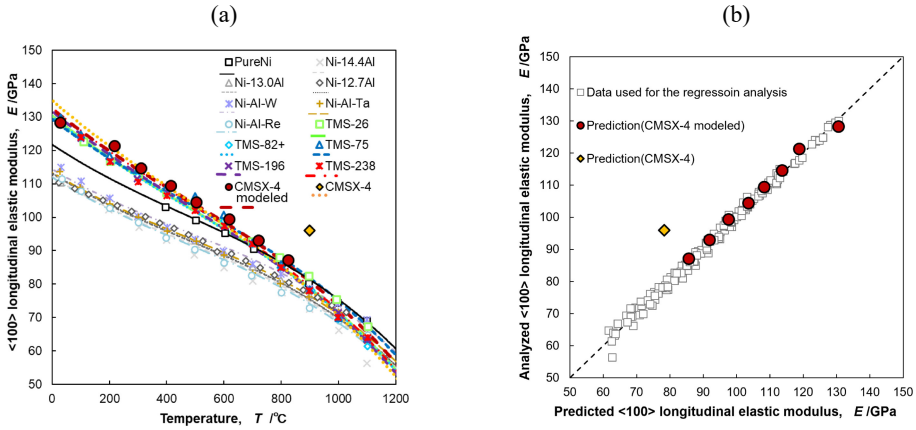

Fig. 15 Temperature dependence of ⟨100⟩ longitudinal elastic modulus of γ phase alloys in Ni-base single-crystal alloys [34]. Date of Ni-12.7 [72], CMSX-4 modeled [73], and CMSX-4 [74] are from references using resonance method by an assumption of anisotropic elastic body. Date of CMSX-4 [74] is from a reference using analysis by an assumption of isotropic elastic body. Copyright 2021 by The Minerals, Metals & Materials Society. Used with permission.

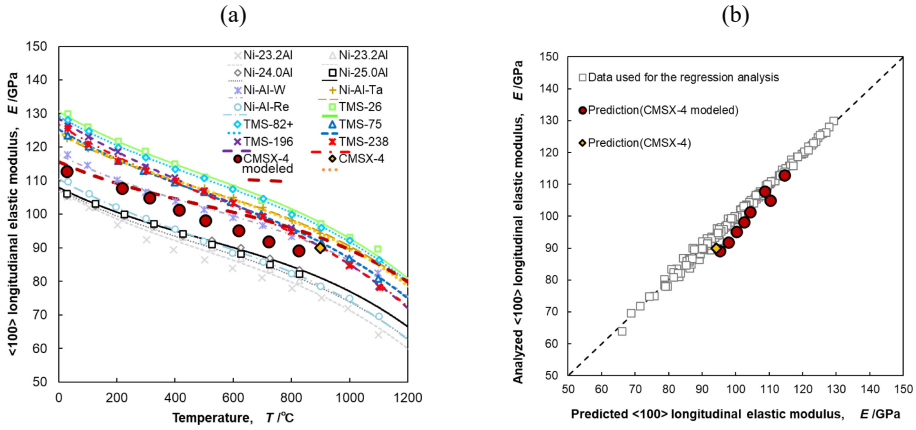

Fig. 16 Temperature dependence of ⟨100⟩ longitudinal elastic modulus of γ′ phase alloys in Ni-base single-crystal alloys [34]. Data of Ni-23.2Al [75], Ni-24.0Al [75], Ni-25.0Al [75], and CMSX-4 modeled [73], are from references using resonance method by an assumption of anisotropic elastic body. Date of CMSX-4 [74] is from a reference using analysis by an assumption of isotropic elastic body. Copyright 2021 by The Minerals, Metals & Materials Society. Used with permission.

regression coefficients D_x, and then the predictive equation of the elastic modulus is obtained.

$$E = D_0 + D_T T + D_{T^2} T^2 + D_{T^3} T^3 + \sum_i (D_{c_i} c_i + D_{A_i} A_i) \tag{4}$$

The referenced elastic modulus of CMSX-4 [74] and CMSX-4 (modeled) [73] in Fig. 15 and Fig. 16 are just used to evaluate the accuracy of the predictive equations and they are not used in the regression analysis. According to Fig. 15 and Fig. 16, established predictive equations show enough good accuracy to reproduce the elastic modulus of CMSXC-4 (modeled) in both of γ and γ′ phases. On the other hand, the predicted elastic modulus of the γ phase in CMSX-4 is far from the referenced values. This is because the referenced elastic modulus of CMSX-4 assumes isotropic elastic bodies, that is different from the assumption of the elastic modulus obtained by the RPR method. This implies that the effect of elastic anisotropy on the elastic modulus of the γ phase is larger than that of the γ′ phase.

Understanding the contributions of the alloying element to the elastic modulus at the target temperature is an important issue for the alloy design. Then, a new regression analysis was conducted to understand the pure effect of the concentration of the alloying element without the consideration of the temperature. First of all, the ⟨100⟩ longitudinal elastic modulus at 900°C was predicted using the alloys which were used in the regression analysis by eq. (4). Next, a new regression analysis based on eq. (5) was conducted using the predicted elastic modulus at 900°C using eq. (4). The regression coefficients obtained by this regression analysis are shown in Fig. 17.

$$E = E_0 + \sum_i D_{c_i} c_i \tag{5}$$

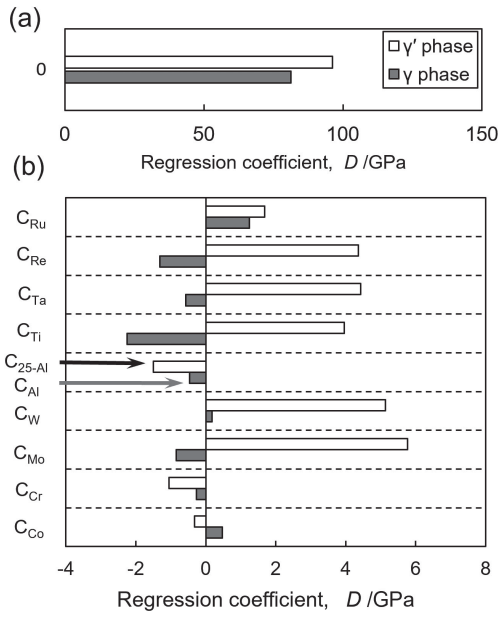

Fig. 17 Regression coefficients of ⟨100⟩ longitudinal elastic modulus at 900°C obtained by regression analysis using eq. (4) [34]. (a) Constant terms, (b) compositional terms. Copyright 2021 by The Minerals, Metals & Materials Society. Used with permission.

Figure 17 indicates that the addition of Re, Ta, Ti, Al, Mo, and Cr to the γ phase decreases the ⟨100⟩ longitudinal elastic modulus, while the addition of Ru, Re, Ta, Ti, Al, W, and Mo increases the ⟨100⟩ longitudinal elastic modulus. Therefore, the addition of Re, Ta, Ti, Al, and Mo could enlarge the elastic misfit positively defined by eq. (3) although estimating the elastic misfit strictly has to consider the partitioning rate of the alloying element between γ and γ′ phases.

6. Future Outlook

The new alloy design approach to control the elastic misfit can be realized if the established predictive equations of the elastic modulus are installed into the ADP which NIMS has been developing. Novel Ni-base single crystal superalloy with superior high-temperature strength could be developed more efficiently in the unpredicted compositions. On the other hand, the predictive equations should continue to be improved in their accuracy by adding more elastic modulus of other Ni-base single crystal alloys.

Established predictive equations of the elastic modulus can be used in various ways except for the alloy design. For instance, predicted elastic modulus can be used in the phase-field simulation and first principal calculation to reproduce more realistic situations as an academic usage. In the case of engineering usage, mechanical parts whose elastic elongation is significant can be more precisely designed adapting to a more realistic situation, using the predicted elastic modulus.

Recently, researchers all over the world are restarting the measurement of the elastic modulus of Ni-base single crystal superalloys more actively [76–80]. Significant progress in the research on the elastic modulus in this field can be expected in near future.

REFERENCES

[1] T. Araki, Y. Aoki, Y. Ueda, A. Sato and M. Hosoya: Research and Development of Advanced Metallic Materials, Ishikawajima-Harima Engineering Review **44** (2004) 266–270.

[2] H. Harada and H. Murakami: Design of Ni-Base superalloys, *Computational Materials Design*, ed. by T. Saito, (Springer Berlin Heidelberg, Berlin, Heidelberg, 1999) pp. 39–70.

[3] H. Harada, T. Yokokawa, K. Kawagishi, T. Kobayashi, Y. Koizumi, M. Sakamoto and M. Yuyama: Materials for High Temperature Turbine Applications: With Actual Practical Use in Mind, Journal of the Gas Turbine Society of Japan **43** (2015) 349–356.

[4] T. Yokokawa, H. Harada, Y. Mori, K. Kawagishi, Y. Koizumi, T. Kobayashi, M. Yuyama and S. Suzuki: Proceedings of the 13th International Symposium on Superalloys, ed. by M. Hardy *et al.*, (Wiley, Hoboken, New Jersey, 2016) pp. 123–130.

[5] T. Yokokawa, H. Harada, K. Kawagishi, T. Kobayashi, M. Yuyama and Y. Takata: Proceedings of the 14th International Symposium on Superalloys, ed. by S. Tin *et al.*, (Springer International Publishing, Cham, 2020) pp. 122–130.

[6] K. Kawagishi, A.C. Yeh, T. Yokokawa, T. Kobayashi, Y. Koizumi and H. Harada: Proceedings of the 12th International Symposium on Superalloys, ed. by E.S. Huron *et al.*, (Wiley, Hoboken, New Jersey, 2012) pp. 189–195.

[7] H. Harada and M. Yamazaki: Alloy Design for γ′ Precipitation Hardening Nickel-base Superalloys Containing Ti, Ta, and W, Tetsu-to-Hagané **65** (1979) 1059–1068.

[8] Y. Koizumi, T. Kobayashi, T. Yokokawa, J. Zhang, M. Osawa, H. Harada, Y. Aoki and M. Arai: Proceedings of the 10th International Symposium on Superalloys, ed. by K.A. Green, (Minerals, Metals & Materials Society, Warrendale, Pennsylvania, 2004) pp. 35–43.

[9] N. Tsuno, A. Sato, K. Tanaka and H. Inui: Evolution of Raft Structure during Creep Deformation of the Ni-Based Single-Crystal Superalloy TMS-138, Adv. Mater. Res. **278** (2011) 19–24.
[10] J.K. Tien and S.M. Copley: The effect of uniaxial stress on the periodic morphology of coherent gamma prime precipitates in nickel-base superalloy crystals, Metall. Trans. **2** (1971) 215–219.
[11] D.D. Pearson, F.D. Lemkey and B.H. Kear: Proceedings of the 4th International Symposium on Superalloys, ed. by J.K. Tien *et al.*, (American Society for Metals, Metal Part, Ohio, 1980) pp. 513–520.
[12] M.V. Nathal and L.J. Ebert: Gamma prime shape changes during creep of a nickel-base superalloy, Scr. Metall. **17** (1983) 1151–1154.
[13] H. Mughrabi, W. Schneider, V. Sass and C. Lang: Proceedings of the 10th International Conference on the Strength of Materials, ed. by H. Oikawa *et al*., (Japan Institute of Metals, Sendai, 1994) pp. 705–708.
[14] T. Murakumo, Y. Koizumi, K. Kobayashi and H. Harada: Proceedings of the 10th International Symposium on Superalloys, ed. by K.A. Green, (Minerals, Metals & Materials Society, Warrendale, Pennsylvania, 2004) pp. 155–162.
[15] A. Epishin, T. Link, U. Brückner and P.D. Portella: Kinetics of the topological inversion of the γ/γ′-microstructure during creep of a nickel-based superalloy, Acta Mater. **49** (2001) 4017–4023.
[16] T. Murakumo, T. Kobayashi, Y. Koizumi and H. Harada: Creep behaviour of Ni-base single-crystal superalloys with various γ′ volume fraction, Acta Mater. **52** (2004) 3737–3744.
[17] M. Nathal, R. MacKay and R. Miner: Influence of precipitate morphology on intermediate temperature creep properties of a nickel-base superalloy single crystal, Metall. Trans. A **20** (1989) 133–141.
[18] J.X. Zhang, J.C. Wang, H. Harada and Y. Koizumi: The effect of lattice misfit on the dislocation motion in superalloys during high-temperature low-stress creep, Acta Mater. **53** (2005) 4623–4633.
[19] J.X. Zhang, T. Murakumo, Y. Koizumi, T. Kobayashi and H. Harada: Slip geometry of dislocations related to cutting of the γ′ phase in a new generation single-crystal superalloy, Acta Mater. **51** (2003) 5073–5081.
[20] J.X. Zhang, T. Murakumo, Y. Koizumi, T. Kobayashi, H. Harada and S. Masaki: Interfacial dislocation networks strengthening a fourth-generation single-crystal TMS-138 superalloy, Metall. Mater. Trans. A **33** (2002) 3741–3746.
[21] R. Field, T. Pollock and W. Murphy: Proceedings of the 7th International Symposium on Superalloys, ed. by S.D. Antolovich *et al*., (Minerals, Metals & Materials Society, Warrendale, Pennsylvania, 1992) pp. 557–566.
[22] J.X. Zhang, H. Harada and Y. Koizumi: New configuration of a [001] superdislocation formed during high-temperature creep in the γ′ phase of a single-crystal superalloy TMS-138, J. Mater. Res. **21** (2006) 647–654.
[23] P.M. Sarosi, R. Srinivasan, G.F. Eggeler, M.V. Nathal and M.J. Mills: Observations of $a\langle 010\rangle$ dislocations during the high-temperature creep of Ni-based superalloy single crystals deformed along the [001] orientation, Acta Mater. **55** (2007) 2509–2518.
[24] A. Sato: Research and development of advanced Ni-based single crystal superalloys and their oxidation-resistant coatings, Ph. D. thesis, Kyoto University, (2006).
[25] T. Saito: Effect of heat treatment on mechanical properties of a high-entropy superalloy, Ph. D. thesis, Waseda University, (2021).
[26] M.V. Nathal, R.A. Mackay and R.G. Garlick: Temperature dependence of γ-γ′ lattice mismatch in Nickel-base superalloys, Mater. Sci. Eng. **75** (1985) 195–205.
[27] L. Müller, T. Link and M. Feller-Kniepmeier: Temperature dependence of the thermal lattice mismatch in a single crystal nickel-base superalloy measured by neutron diffraction, Scr. Metall. Mater. **26** (1992) 1297–1302.
[28] M.V. Nathal and R.A. Mackay: The stability of lamellar γ-γ′ structures, Mater. Sci. Eng. **85** (1987) 127–138.
[29] M. Doi and T. Miyazaki: Proceedings of the 5th International Symposium on Superalloys, ed. by M. Gell *et al*., (Metallurgical Society of AIME, Warrendale, Pennsylvania, 1984) pp. 543–552.
[30] T. Miyazaki, H. Imamura, H. Mori and T. Kozakal: Theoretical and experimental investigations on elastic interactions between γ′-precipitates in a Ni-Al alloy, J. Mater. Sci. **16** (1981) 1197–1203.
[31] W.C. Johnson and P.W. Voorhees: Elastic interaction and stability of misfitting cuboidal inhomogeneities, J. Appl. Phys. **61** (1987) 1610–1619.
[32] A. Pineau: Influence of uniaxial stress on the morphology of coherent precipitates during coarsening—elastic energy considerations, Acta Metall. **24** (1976) 559–564.
[33] T. Ichitsubo, D. Koumoto, M. Hirao, K. Tanaka, M. Osawa, T. Yokokawa and H. Harada: Rafting mechanism for Ni-base superalloy under external stress: elastic or elastic–plastic phenomena?, Acta Mater. **51** (2003) 4033–4044.
[34] T. Saito, M. Osawa, T. Yokokawa, H. Harada, T. Kobayashi, K. Kawagishi and S. Suzuki: Proceedings of the 14th International Symposium on Superalloys, ed. by S. Tin *et al.*, (Springer International Publishing, Cham, 2020) pp. 312–323.
[35] J.D. Eshelby: Proceedings of the Royal Society of London Series A Mathematical and Physical Sciences, Vol. 241, (The Royal Society of London, London, 1957) pp. 376–396.
[36] T.M. Pollock and A.S. Argon: Directional coarsening in nickel-base single crystals with high volume fractions of coherent precipitates, Acta Metall. Mater. **42** (1994) 1859–1874.
[37] H. Gabrisch, D. Mukherji and R.P. Wahi: Deformation-induced dislocation networks at the γ-γ′ interfaces in the single-crystal superalloy SC16: A mechanism-based analysis, Philos. Mag. A **74** (1996) 229–249.
[38] H. Gabrisch and D. Mukherji: Character of dislocations at the γ/γ′ interfaces and internal stresses in nickel-base superalloys, Acta Mater. **48** (2000) 3157–3167.
[39] N. Zhou, C. Shen, M.J. Mills and Y. Wang: Phase field modeling of channel dislocation activity and γ′ rafting in single crystal Ni–Al, Acta Mater. **55** (2007) 5369–5381.
[40] N. Zhou, C. Shen, P. Sarosi, M. Mills, T. Pollock and Y. Wang: γ′ rafting in single crystal blade alloys: A simulation study, Mater. Sci. Technol. **25** (2009) 205–212.
[41] I.L. Svetlov, B.A. Golovko, A.I. Epishin and N.P. Abalakin: Diffusional mechanism of γ′-phase particles coalescence in single crystals of nickel-base superalloys, Scr. Metall. Mater. **26** (1992) 1353–1358.
[42] M. Saito, T. Aoyama, K. Hidaka, H. Tamaki, T. Ohashi, S. Nakamura and T. Suzuki: Concentration profiles and the rafting mechanism of Ni base superalloys in the initial stage of high temperature creep tests, Scr. Mater. **34** (1996) 1189–1194.
[43] T. Ohashi, K. Hidaka and S. Imano: Elastic stress in single crystal Ni-base superalloys and the driving force for their microstructural evolution under high temperature creep conditions, Acta Mater. **45** (1997) 1801–1810.
[44] J.X. Zhang, T. Murakumo, Y. Koizumi and H. Harada: The influence of interfacial dislocation arrangements in a fourth generation single crystal TMS-138 superalloy on creep properties, J. Mater. Sci. **38** (2003) 4883–4888.
[45] T.P. Gabb, S.L. Draper, D.R. Hull, R.A. Mackay and M.V. Nathal: The role of interfacial dislocation networks in high temperature creep of superalloys, Mater. Sci. Eng. A **118** (1989) 59–69.
[46] M. Osawa, H. Shiraishi, T. Yokokawa, H. Harada and T. Kobayashi: Proceedings of the 10th International Symposium on Superalloys, ed. by K.A. Green, (Minerals, Metals & Materials Society, Warrendale, Pennsylvania, 2004) pp. 977–985.
[47] P. Kontis, Z. Li, D.M. Collins, J. Cormier, D. Raabe and B. Gault: The effect of chromium and cobalt segregation at dislocations on nickel-based superalloys, Scr. Mater. **145** (2018) 76–80.
[48] M.V. Nathal and L.J. Ebert: Elevated temperature creep-rupture behavior of the single crystal nickel-base superalloy NASAIR 100, Metall. Trans. A **16** (1985) 427–439.
[49] G. Eggeler and A. Dlouhy: On the formation of ⟨010⟩-dislocations in the γ′-phase of superalloy single crystals during high temperature low stress creep, Acta Mater. **45** (1997) 4251–4262.
[50] T. Link, A. Epishin, M. Klaus, U. Brückner and A. Reznicek: ⟨100⟩ Dislocations in nickel-base superalloys: Formation and role in creep deformation, Mater. Sci. Eng. A **405** (2005) 254–265.
[51] R. Srinivasan, G.F. Eggeler and M.J. Mills: γ′-cutting as rate-controlling recovery process during high-temperature and low-stress creep of superalloy single crystals, Acta Mater. **48** (2000) 4867–4878.
[52] C. Kohler, T. Link and A. Epishin: Dissociation of $a\langle 100\rangle$ edge superdislocations in the γ′-phase of nickel-base superalloys, Philos.

Mag. **86** (2006) 5103–5121.
[53] R. Srinivasan, M.V. Nathal, M.S. Daw, G.F. Eggeler and M.J. Mills: Proceedings of the Third International Symposium on Structural Intermetallics, ed. by K.J. Hemker *et al.*, (Minerals, Metals & Materials Society, Warrendale, Pennsylvania, 2001) pp. 423–430.
[54] T. Yamagata, H. Harada, S. Nakazawa, M. Yamazaki and Y. Nakagawa: Proceedings of the 5th International Symposium on Superalloys, ed. by M. Gell *et al.*, (Metallurgical Society of AIME, Warrendale, Pennsylvania, 1984) pp. 157–165.
[55] K. Tanaka, T. Ichitsubo, K. Kishida, H. Inui and E. Matsubara: Elastic instability condition of the raft structure during creep deformation in nickel-base superalloys, Acta Mater. **56** (2008) 3786–3790.
[56] Y. Tsukada, Y. Murata, T. Koyama and M. Morinaga: Phase-Field Simulation on the Formation and Collapse Processes of the Rafted Structure in Ni-Based Superalloys, Mater. Trans. **49** (2008) 484–488.
[57] P. Caron, C. Ramusat and F. Diologent: Proceedings of the 11th International Symposium on Superalloys, ed. by R.C. Reed *et al.*, (Minerals, Metals & Materials Society, Warrendale, Pennsylvania, 2008) pp. 159–167.
[58] S. Antonov, Y. Zheng, J.M. Sosa, H.L. Fraser, J. Cormier, P. Kontis and B. Gault: Plasticity assisted redistribution of solutes leading to topological inversion during creep of superalloys, Scr. Mater. **186** (2020) 287–292.
[59] P.J. Warren, A. Cerezo and G.D.W. Smith: An atom probe study of the distribution of rhenium in a nickel-based superalloy, Mater. Sci. Eng. A **250** (1998) 88–92.
[60] H. Murakami, P.J. Warren and H. Harada: Proceedings of the Third International Charles Parsons Turbine Conference, (Institute of Materials, Newcastle upon Tyne, 1995) p. 343.
[61] R.A. Mackay and J.E. Lynn: Proceedings of the 5th International Symposium on Superalloys, ed. by M. Gell *et al.*, (Metallurgical Society of AIME, Warrendale, Pennsylvania, 1984) pp. 135–144.
[62] T. Hino, T. Kobayashi, Y. Koizumi, H. Harada and T. Yamagata: Proceedings of the 9th International Symposium on Superalloys, ed. by T.M. Pollock *et al.*, (Minerals, Metals & Materials Society, Warrendale, Pennsylvania, 2000) pp. 729–736.
[63] P. Caron and T. Khan: Improvement of Creep strength in a nickel-base single-crystal superalloy by heat treatment, Mater. Sci. Eng. **61** (1983) 173–184.
[64] R.A. MacKay and L.J. Ebert: The development of γ-γ′ lamellar structures in a nickel-base superalloy during elevated temperature mechanical testing, Metall. Trans. A **16** (1985) 1969–1982.
[65] M.V. Nathal and L.J. Ebert: The influence of cobalt, tantalum, and tungsten on the microstructure of single crystal nickel-base superalloys, Metall. Trans. A **16** (1985) 1849–1862.
[66] T. Kobayashi, H. Harada and J. Zhang: Influence of Heat Treatment on Microstructure and Mechanical Properties of a 1st Generation Single-Crystal Superalloy, J. Japan Inst. Metals **70** (2006) 47–50.
[67] H. Harada, T. Ohno, T. Yamagata, T. Yokokawa and M. Yamazaki: Proceedings of the 6th International Symposium on Superalloys, ed. by D.N. Duhl *et al.*, (Minerals, Metals & Materials Society, Warrendale, Pennsylvania, 1988) pp. 733–742.
[68] H.H. Demarest: Cube-Resonance Method to Determine the Elastic Constants of Solids, J. Acoust. Soc. Am. **49** (1971) 768–775.
[69] I. Ohno: Free vibration of a rectangular parallelepiped crystal and its application to determination of elastic constants of orthorhombic crystals, J. Phys. Earth **24** (1976) 355–379.
[70] Y. Hideyuki and K. Masahiro: Determination of elastic constants of single crystals with cubic symmetry by the rectangular parallelepiped resonance method, J. Phys. Chem. Solids **52** (1991) 723–729.
[71] S. Siegel and S.L. Quimby: The Variation of Young's Modulus with Magnetization and Temperature in Nickel, Phys. Rev. **49** (1936) 663–670.
[72] S.V. Prikhodko, J.D. Carnes, D.G. Isaak and A.J. Ardell: Elastic Constants of a Ni-12.69 AT. % Al Alloy From 295 to 1300 K, Scr. Mater. **38** (1997) 67–72.
[73] D. Siebörger, H. Knake and U. Glatzel: Temperature dependence of the elastic moduli of the nickel-base superalloy CMSX-4 and its isolated phases, Mater. Sci. Eng. A **298** (2001) 26–33.
[74] D. Dye, J. Coakley, V.A. Vorontsov, H.J. Stone and R.B. Rogge: Elastic moduli and load partitioning in a single-crystal nickel superalloy, Scr. Mater. **61** (2009) 109–112.
[75] S.V. Prikhodko, H. Yang, A.J. Ardell, J.D. Carnes and D.G. Isaak: Temperature and composition dependence of the elastic constants of Ni_3Al, Metall. Mater. Trans. A **30** (1999) 2403–2408.
[76] A. Epishin, B. Fedelich, M. Finn, G. Künecke, B. Rehmer, G. Nolze, C. Leistner, N. Petrushin and I. Svetlov: Investigation of Elastic Properties of the Single-Crystal Nickel-Base Superalloy CMSX-4 in the Temperature Interval between Room Temperature and 1300 °C, Crystals **11** (2021) 152.
[77] B.R. Goodlet, S.P. Murray, B. Bales, J. Rossin, C.J. Torbet and T.M. Pollock: Temperature dependence of single crystal elastic constants in a CoNi-Base alloy: A new methodology, Mater. Sci. Eng. A **803** (2021) 140507.
[78] O.M. Horst, D. Schmitz, J. Schreuer, P. Git, H. Wang, C. Körner and G. Eggeler: Thermoelastic properties and γ′-solvus temperatures of single-crystal Ni-base superalloys, J. Mater. Sci. **56** (2021) 7637–7658.
[79] B.R. Goodlet, L. Mills, B. Bales, M.-A. Charpagne, S.P. Murray, W.C. Lenthe, L. Petzold and T.M. Pollock: Elastic Properties of Novel Co- and CoNi-Based Superalloys Determined through Bayesian Inference and Resonant Ultrasound Spectroscopy, Metall. Mater. Trans. A **49** (2018) 2324–2339.
[80] K. Demtröder, G. Eggeler and J. Schreuer: Influence of microstructure on macroscopic elastic properties and thermal expansion of nickel-base superalloys ERBO/1 and LEK94, Materialwiss. Werkstofftech. **46** (2015) 563–576.